AD-A126 673 ACOUSTICAL INTERFEROMETRY(U) ARMY MISSILE COMMAND 1/1
REDSTONE ARSENAL AL GROUND EQUIPMENT AND MISSILE
STRUCTURES DIRECTORATE W F SWINSON MAR 81
UNCLASSIFIED DRSMI/RL-81-3-TR SBI-AD-E950 371 F/G 20/10 NL

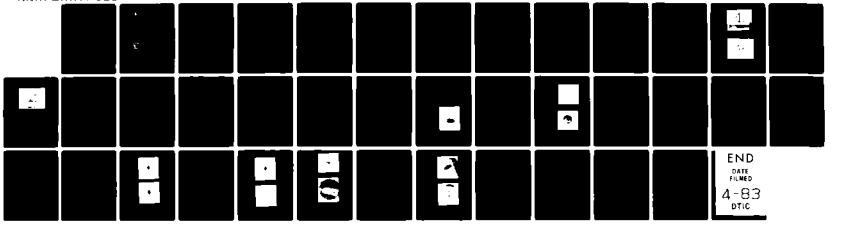

END
DATE FILMED
4-83
DTIC

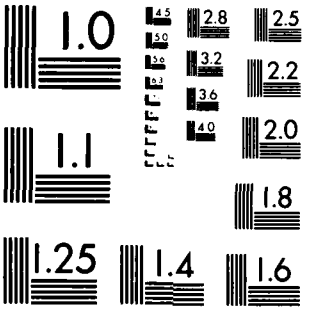

MICROCOPY RESOLUTION TEST CHART
NATIONAL BUREAU OF STANDARDS 1963 A

Army mat Cmd. RL-TR-81-3

SMI-RL (1)

ALE 950 371

AD A126673

TECHNICAL REPORT RL-81-3

ACOUSTICAL INTERFEROMETRY

W. F. Swinson
for
Ground Equipment and Missile Structures Directorate
US Army Missile Laboratory

MARCH 1981

U.S. ARMY MISSILE COMMAND
Redstone Arsenal, Alabama 35898

Approved for public release; distribution unlimited.

DTIC FILE COPY

DTIC ELECTE APR 8 1983

83 04 08 062 A

SMI FORM 1021, 1 JUL 79 PREVIOUS EDITION IS OBSOLETE

DISPOSITION INSTRUCTIONS

DESTROY THIS REPORT WHEN IT IS NO LONGER NEEDED. DO NOT RETURN IT TO THE ORIGINATOR.

DISCLAIMER

THE FINDINGS IN THIS REPORT ARE NOT TO BE CONSTRUED AS AN OFFICIAL DEPARTMENT OF THE ARMY POSITION UNLESS SO DESIGNATED BY OTHER AUTHORIZED DOCUMENTS.

TRADE NAMES

USE OF TRADE NAMES OR MANUFACTURERS IN THIS REPORT DOES NOT CONSTITUTE AN OFFICIAL INDORSEMENT OR APPROVAL OF THE USE OF SUCH COMMERCIAL HARDWARE OR SOFTWARE.

SECURITY CLASSIFICATION OF THIS PAGE (When Data Entered)

REPORT DOCUMENTATION PAGE		READ INSTRUCTIONS BEFORE COMPLETING FORM
1. REPORT NUMBER TR-RL-81-3	2. GOVT ACCESSION NO.	3. RECIPIENT'S CATALOG NUMBER
4. TITLE (and Subtitle) Acoustical Interferometry		5. TYPE OF REPORT & PERIOD COVERED Technical Report
		6. PERFORMING ORG. REPORT NUMBER
7. AUTHOR(s) Weldon F. Swinson		8. CONTRACT OR GRANT NUMBER(s) DAlL162303A214
9. PERFORMING ORGANIZATION NAME AND ADDRESS Commander US Army Missile Command ATTN: DRSMI-RL Redstone Arsenal, Alabama 35898		10. PROGRAM ELEMENT, PROJECT, TASK AREA & WORK UNIT NUMBERS AMCMS 6123032140911
11. CONTROLLING OFFICE NAME AND ADDRESS Commander US Army Missile Command ATTN: DRSMI-RPT Redstone Arsenal, Alabama 35898		12. REPORT DATE March 1981 13. NUMBER OF PAGES 34
14. MONITORING AGENCY NAME & ADDRESS(if different from Controlling Office)		15. SECURITY CLASS. (of this report) unclassified 15a. DECLASSIFICATION/DOWNGRADING SCHEDULE

16. DISTRIBUTION STATEMENT (of this Report)

Approved for public release; distribution unlimited.

17. DISTRIBUTION STATEMENT (of the abstract entered in Block 20, if different from Report)

18. SUPPLEMENTARY NOTES

This work was accomplished through the Laboratory Research Cooperative Program (LRCP) between Dr. W. F. Swinson of Auburn University and the US Army Missile Command.

19. KEY WORDS (Continue on reverse side if necessary and identify by block number)

Acoustical Holography
Acoustical Speckle Interferometry
Flaw Detection & Quantification
Acoustical Interferometry

20. ABSTRACT (Continue on reverse side if necessary and identify by block number)

This report documents work in acoustical interferometry. Theory and experimental examples are presented to illustrate the technique.

DD FORM 1 JAN 73 1473 EDITION OF 1 NOV 65 IS OBSOLETE Uncl

SECURITY CLASSIFICATION OF THIS PAGE (When Data Entered)

CONTENTS

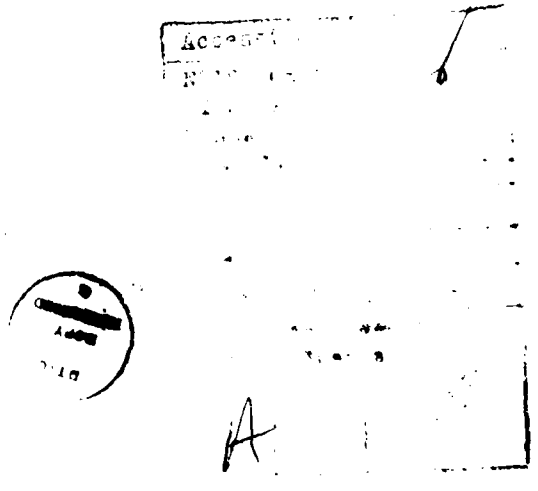

LIST OF ILLUSTRATIONS

I. INTRODUCTION

Real-time acoustical interferometry is one of the most promising techniques in experimental mechanics. Engineers need stress and strain information both on the surface of an object as well as the interior to locate "critical points" (points of highest stress) for structural evaluation of any design. Acoustic waves have the potential to give this information. They are nondestructive, do not alter the performance of what is being examined, and carry information about every point in an object. No other technique has such a broad range of possibilities as does acoustic interferometry. Presently acoustic waves are helpful in locating flaws and cracks in objects being tested, but it also has the potential of gathering and signaling information related to strain (or stress) at critical points. Because of this important potential, development work is needed in acoustic interferometry.

II. REAL-TIME ACOUSTICAL HOLOGRAPHY THEORY

Theory for acoustical holography is somewhat complicated. Consider two ultrasonic waves intersecting at a liquid-air surface. These waves are usually represented as continuous longitudinal waves, but in the usual holographic systems are intermittent waves. Further, the disturbance at a point on the surface is treated as a linear sum of the two waves, but in fact this is complicated by the presence of surface waves intersecting the liquid-air surface and further complicated due to reflecting longitudinal waves interfering with incoming longitudinal waves. Even though these complications exist a theory can be developed that does assist in predicting effects and helps in understanding the results.

The reference wave is assumed to be a plane wave and the longitudinal acoustic disturbance is given as the real part of (see Figure 1)

$$\bar{P}_{AR} = \bar{P}_R e^{i(\omega_A t + \phi_{RO} - \frac{2\pi}{\lambda_A} y \sin \theta_R)} \tag{1}$$

where

$\bar{P}_R$ = magnitude of the acoustic disturbance

ω_A = acoustic frequency

t = time

ϕ_{RO} = phase of the reference beam at "0"

λ_A = acoustic longitudinal wave

The object wave, while initially a plane wave, has been distorted due to the object and is represented as

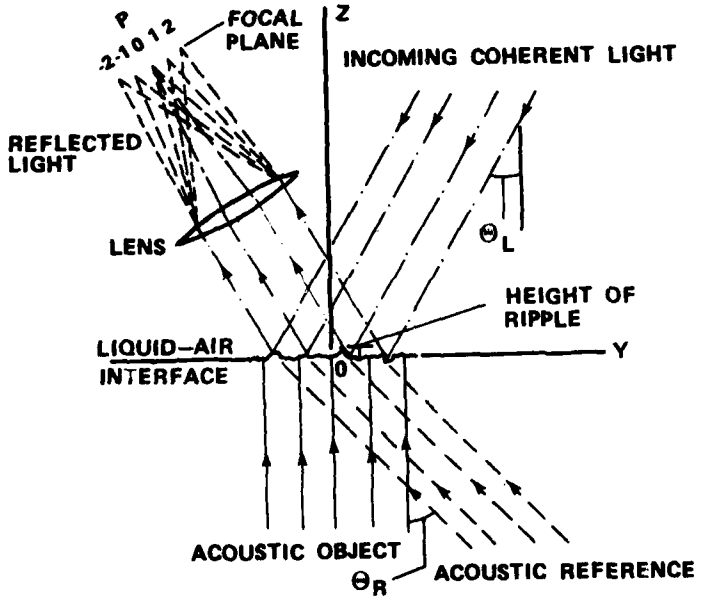

Figure 1. Interfering waves.

$$\bar{P}_{AO} = \bar{P}_o \, e^{i(\omega_A t + \phi_o)} \tag{2}$$

where

$\bar{P}_o$ = the magnitude of the longitudinal object wave and is an unknown function of x and y,

ϕ_o = the phase of the object wave and likewise is an unknown function of x and y.

The acoustic disturbance at the surface is

$$\bar{P} = \bar{P}_{AR} + \bar{P}_{AO} \tag{3}$$

while the intensity which manifest itself as the "height" of the ripple at the liquid-air interface is

$$I = C_1 \, (\bar{P} \cdot \bar{P}^*)$$

or

$$I = C_1 \, (\bar{P}_{AR} \cdot \bar{P}_{AR}^* + \bar{P}_{AR} \cdot \bar{P}_{AO}^* + \bar{P}_{AR}^* \cdot \bar{P}_{AO} + \bar{P}_{AO} \cdot \bar{P}_{AO}^* \tag{4}$$

where

C_1 = a proportionality constant and

$()^*$ = the complex conjugate.

In expanded form

$$I = C_1 \left[P_R^2 + P_O^2 + P_R P_O \, (e^{i(\phi_o - \phi_{RO} + \frac{2\pi}{\lambda_A} y \sin \theta_R)} \right.$$

$$\left. + e^{-i(\phi_o - \phi_{RO} + \frac{2\pi}{\lambda_A} y \sin \theta_R)}) \right] \tag{5}$$

or

$$I = C_1 \left[P_R^2 + P_O^2 + 2 P_R P_O \cos \, (\phi_O - \phi_{RO} + \frac{2\pi}{\lambda_A} y \sin \theta_R) \right] \; .$$

The ripple surface at the liquid-air interface modulates the path length of the

coherent light source. If the light beam angle (θ_L) is kept small the optical path length difference can be described as 2Z, or since Z is taken as corresponding to the acoustic intensity at the surface

$$2Z = 2I. \tag{6}$$

Next, the optical disturbance from a small region (dx dy) or dA_1, being collected by the lens (Figure 1) is

$$d\bar{E} = \bar{A}e^{i\left\{\omega_L t + \phi_L + \frac{4\pi}{\lambda_L} C_1\left[P_R^2 + P_O^2 + 2 P_R P_O \cos\left(\phi_O - \phi_{RO} + \frac{2\pi}{\lambda_A} y \sin \phi_R\right)\right]\right\}} dA_1. \tag{7}$$

The optical disturbance at a point P in the focal plane is

$$\bar{E} = \bar{A}e^{i(\omega_L t + \phi_L)} \int_{A_1} e^{i\frac{4\pi}{\lambda_L} C_1\left[P_R^2 + P_O^2 + 2 P_R P_O \cos\left(\phi_O - \phi_{RO} + \frac{2\pi}{\lambda_A} y \sin \theta_R\right)\right]} dA_1 \tag{8}$$

where A_1 is the acoustic image area.

In assuming that the maximum amplitude of P_R and P_O are essentially constant over the acoustic image area, the optical disturbance can be further simplified

$$\bar{E} = \bar{A}e^{i\left[\omega_L t + \phi_L + \frac{4\pi}{\lambda_L} C_1 (P_R^2 + P_O^2)\right]} \int_{A_1} e^{i\frac{8\pi}{\lambda_L} C_1 P_R P_O \cos\left(\phi_O - \phi_{RO} + \frac{2\pi}{\lambda_A} y \sin \theta_R\right)} dA_1 \tag{9}$$

Using the identity

$$e^{i x \cos\theta} = J_o(X) + 2iJ_1(X)\cos\theta - 2J_2(X)\cos 2\theta + \cdots$$

$$= J_o(X) + i J_1(X)\left[e^{i\theta} + e^{-i\theta}\right] - J_2(X)\left[e^{i2\theta} + e^{i2\theta}\right] + \cdots \tag{10}$$

$$\bar{E} = \bar{A} e^{i\left[\omega_L t + \phi_L + \frac{4\pi}{\lambda_L} C_1 (P_R^2 + P_O^2)\right]} \int_{A_1} \left\{ J_o\left(\frac{8\pi}{\lambda_L} C_1 P_R P_O\right) \right.$$

$$+ 2iJ_1\left(\frac{8\pi}{\lambda_L} C_1 P_R P_O\right) \left[e^{i(\phi_o - \phi_{RO} + \frac{2\pi}{\lambda_A} y \sin\theta_R)} \right.$$

$$\left. \left. + e^{-i(\phi_o - \phi_{RO} + \frac{2\pi}{\lambda_A} y \sin\theta_R)} \right] + \cdots \right\} dA_1 , \qquad (11)$$

where the J ( ) terms represent Bessel Functions. The integrals represent diffraction orders and can be observed separately by blocking out the undesired orders at the focal plane. The zero order is

$$\bar{E}_o = \bar{A}\, e^{i\left[\omega_L t + \phi_L + \frac{4\pi}{\lambda_L} C_1 (P_R^2 + P_O^2)\right]} J_o\left(\frac{8\pi}{\lambda_L} C_1 P_O P_R\right) A_1 \qquad (12)$$

and the intensity is

$$I_o = A^2 \left[J_o\left(\frac{8\pi}{\lambda_L} C_1 P_O P_R\right)\right]^2 A_1^2 . \qquad (13)$$

An interpretation of this says that over the area of the acoustic image, A_1, a modulated intensity represented in $J_o(\frac{8\pi}{\lambda_L} C_1 P_O P_R)$ will be observed. An example of this is shown in Figure 2. As can be seen from Equation (12), the zero order beam does not contain information about the phase of the acoustic object beam and is not a true hologram, although it is sometimes classed as such. It is further noted that if the acoustic reference beam goes to zero, leaving only the object beam, basically the same information is available.

The disturbance contained in the first order beam is

$$\bar{E}_1 = \bar{A} e^{i\left[\omega_L t + \phi_L + \frac{4\pi}{\lambda_L} C_1 (P_R^2 + P_O^2)\right]} \int_{A_1} 2iJ_1\left(\frac{8\pi}{\lambda_L} C_1 P_R P_O\right)$$

$$e^{i(\phi_o - \phi_{RO} + \frac{2\pi}{\lambda_A} y \sin\theta_R)} dA_1 \qquad (14)$$

and contains information about the amplitude and the phase of the object beam; there is a true hologram. This is a little more apparent when the argument of

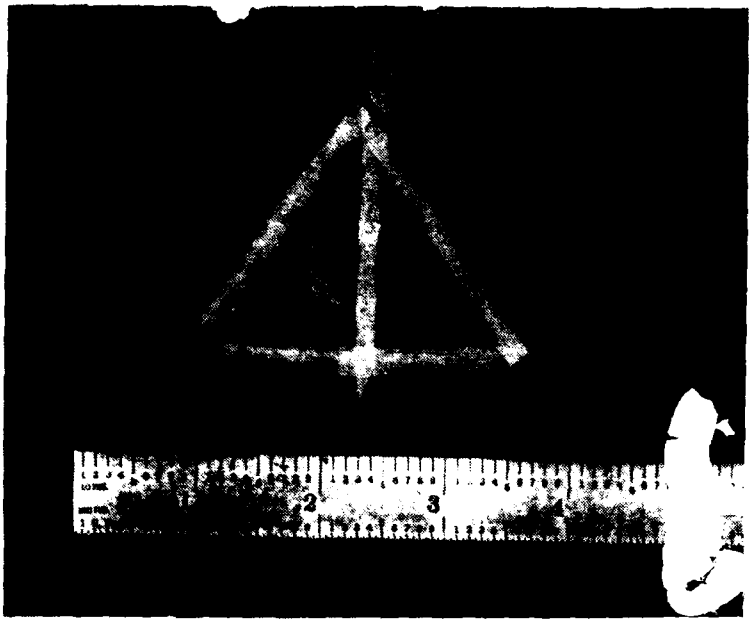

Figure 2a. Object mounted on 1/8-inch Plexiglas.

Figure 2b. Zero-order image of object.

J_1 is assumed small, in which case

$$J_1 \left(\frac{8\pi}{\lambda_L} C_1 P_R P_O\right) \Rightarrow \frac{4\pi}{\lambda_L} C_1 P_R P_O \cdot \tag{15}$$

Thus,

$$\bar{E}_1 = Ae^{i\left[\omega_L t + \phi_L - \phi_{RO} + \frac{4\pi}{\lambda_L} C_1 (P_R^2 + P_O^2)\right]} e^{i\frac{8\pi}{\lambda_L} C_1 P_R}$$

$$\int_{A_1} P_O e^{i(\phi_o)} e^{i\frac{2\pi}{\lambda_A} y \sin\theta_R} dA_1 \cdot \tag{16}$$

The product $P_O e^{i\phi_o}$ in the integral of Equation (16) contains the original acoustic object information and is modulated by $e^{i\frac{2\pi}{\lambda_A} y \sin\theta_R}$. The other terms of Equation (16) can be considered as representing background noise. An example of this first-order acoustic hologram is shown in Figure 3. It can be observed from Equation (16) that if the reference beam goes to zero the first order and above diffraction orders disappear. Also, it can be reasoned that if θ_R is made small the more closely the integral of Equation (16) matches the original object beam. This effect was observed in practice.

III. ACOUSTICAL INTERFEROMETRY WITH HOLOGRAPHY

Since the first-order diffraction (in fact, all diffraction orders except zero) contain information about the original object beam to include amplitude and phase, a hologram can be recorded on film using any one of these orders and an external reference beam. The concept has possibilities in that double exposed holograms are feasible and can yield quantitative information about the object displacement under load. A few remarks about the development that follows are in order. The optical disturbance at a point is the sum of contributions from all radiating points as can be seen, for example, by the integral of Equation (8). The result can be developed using convolution functional analysis. Another way to develop the result is carry along the integrals. Still another way of arriving at the results is by redefining the integral as a new function with a magnitude and phase representing all contributions of the radiating sources. This is similar to representing a series of harmonic functions by a single harmonic function. This latter approach is used in the following development. The approach is reasonably straightforward and developments from past work are more easily recognized.

To help relieve the inconvenience of keeping up with so many terms, let

Figure 3. First-order acoustic hologram.

$$\bar{A}' = \bar{A}\,\frac{8\pi}{\lambda_L}\,C_1 P_R \ ,$$

and

$$e^{i\phi'_L} = e^{i\left[\phi_L + \frac{4\pi}{\lambda_L} C_1 (P_R^2 + P_O^2) - \phi_{RO}\right]} \ ,$$

thus, the optical disturbance at a point on a film (see Figure 4) is

$$\bar{E}_1 = \bar{A}'\, e^{i(\omega_L t + \phi'_L)} \int_{A_1} i\, P_O e^{i(\phi_O)}\, e^{i\frac{2\pi}{\lambda_A} y \sin\theta_R}\, dA_1 \qquad (17)$$

The reference beam is

$$\bar{E}_R = \bar{A}_R\, e^{i(\omega_L t + \phi_{LR})} \ . \qquad (18)$$

As illustrated in Figure 4, the optical disturbance on the hologram film is

$$\bar{E} = \bar{E}_1 + \bar{E}_R$$

or

$$\bar{E} = \bar{A}'\, e^{i(\omega_L t + \phi'_L)} \int_{A_1} i\, P_O e^{i\phi_O}\, e^{i\frac{2\pi}{\lambda_A} y \sin\theta_R}\, dA_1$$

$$+ \bar{A}_R\, e^{i(\omega_L t + \phi_{LR})} \ . \qquad (19)$$

As usual, multiplying by the complex conjugate

$$\bar{E}^* = -\bar{A}'\, e^{i(\omega_L t + \phi'_L)} \int_{A_1} i\, P_O e^{-i\phi_O}\, e^{-i\frac{2\pi}{\lambda_A} y \sin\theta_R}\, dA_1$$

$$+ \bar{A}_R\, e^{i(\omega_L t + \phi_{LR})} \qquad (20)$$

yields the intensity as

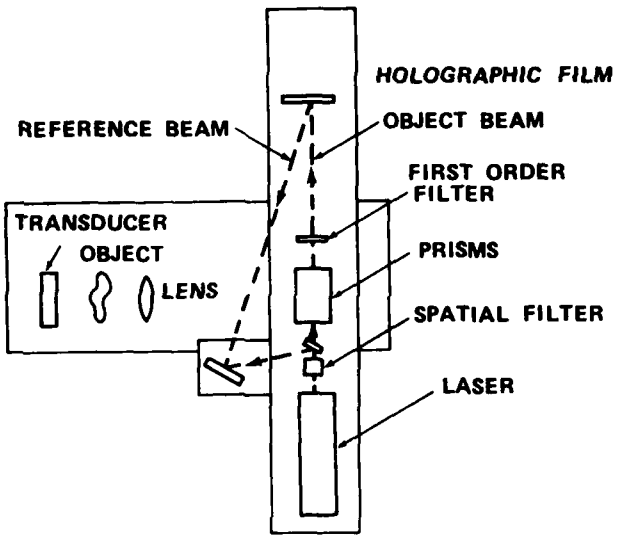

Figure 4. Hologram arrangement.

$$I = (A')^2 P_0^2 A_1 + A_R^2 + A_R A' e^{i(\phi_L' - \phi_{LR})} i\int_{P_0} e^{i(\phi_0 + \frac{2\pi}{\lambda_A} y \sin\theta_R)} dA_1$$

$$- A_R A' e^{-i(\phi_L' - \phi_{LR})} i\int_{A_1} P_0 e^{-i(\phi_0 + \frac{2\pi}{\lambda_A} y \sin\theta_R)} dA_1 . \qquad (21)$$

The film exposure is the product of intensity and time (It). On reconstruction, the optic disturbance transmitted through the film is approximated as

$$dE = I E_R dA_1 \qquad (22)$$

at any point. Thus, at the focal point the optical disturbance is

$$\bar{E} = \int_{A_{FILM}} \left[(A')^2 P_0^2 A_1 + A_R^2\right] \bar{A}_R e^{i(\omega t + \phi_{LR})} dA_{FILM}$$

$$+\int_{A_{FILM}} A_R A' \bar{A}_R i \int_e i(\phi_L' + \phi_0 + \frac{2\pi}{\lambda_A} y \sin\theta_R) P_0 dA_1 dA_{FILM} \qquad (23)$$

$$-\int_{A_{FILM}} A_R A' \bar{A}_R i \int_{A_1} P_0 e^{-i(\phi_L' - 2\phi_{LR} + \phi_0 + \frac{2\pi}{\lambda_A} y \sin\theta_R)} dA_1 dA_{FILM} .$$

The first term of Equation (23) represents the undiffracted wave front. The second term contains information about the object and is commonly called a virtual image wave front. The third term contains information about the object and is classed as a real image wave front. The wave fronts should be separated as with usual off-axis holography.

By way of application consider a double exposed hologram, so a hologram is taken of an object, the object displaced to change the phase, and a second hologram is superimposed on the first. The intensity distribution is

$$I = \left\{(A')^2 P_0^2 A_1 + A_R^2 + A_R A' e^{i(\phi_L' - \phi_{LR})} i\int_{A_1} P_0 e^{i(\phi_o + \frac{2\pi}{\lambda_A} y \sin\theta_R)} dA_1 \right.$$

$$\left. - A_R A' e^{-i(\phi_L' - \phi_{LR})} i\int_{A_1} P_0 e^{-i(\phi_o - \frac{2\pi}{\lambda_A} y \sin\theta_R)} dA_1 \right\}$$

$$+ (A')^2 P_0^2 A_1 + A_R^2 + A_R A' e^{i(\phi_L' - \phi_{LR})}$$

$$\cdot i\int_{A_1} P_0 e^{i(\phi_o + \Delta\phi_o + \frac{2\pi}{\lambda_A} y \sin\theta_R)} dA_1$$

$$- A_R A' e^{-i(\phi_L' - \phi_{LR})} i\int_{A_1} P_0 e^{-i(\phi_o + \Delta\phi_o + \frac{2\pi}{\lambda_A} y \sin\theta_R)} dA_1 \qquad (24)$$

where

$\Delta\phi_o$ = the object phase change due to displacement of object.

On reconstruction of the double exposed hologram with the reference beam, the optical disturbance at a point is

$$\bar{E} = \int_{A_{FILM}} 2 \left\{ (A')^2 P_0^2 A_1 + A_R^2 \right\} \bar{A}_R e^{i(\omega_L t + \phi_{LR})} dA_{FILM}$$

$$+ \bar{A}_R \int_{A_{FILM}} A_R A' e^{i(\phi_L' + \omega_L t)} i\int_{A_1} P_0 e^{i(\phi_o + \frac{2\pi}{\lambda_A} y \sin\theta_R)}$$

$$\cdot (1 + e^{i\Delta\phi_o}) \, dA_1 dA_{FILM}$$

$$- \bar{A}_R \int_{A_{FILM}} A_R A' e^{-i(\phi_L' - 2\phi_{LR} - \omega_L t)} i\int_{A_1} P_0 e^{-i(\phi_o + \frac{2\pi}{\lambda_A} y \sin\theta_R)}$$

$$\cdot (1 + e^{-i\Delta\phi_o}) \, dA_1 dA_{FILM} \qquad (25)$$

The second term is the virtual image distrubance. The intensity of the virtual image is found by multiplying by the complex conjugate or

$$I = \bar{A}_R \int_{A_{FILM}} A_R A' e^{i(\phi_L' + \omega_L t)} \; i \int_{A_1} P_O e^{i(\phi_O + \frac{2\pi}{\lambda_A} y \sin \theta_R)}$$

$$\cdot (1+e^{i\Delta\phi_O}) \, dA_1 dA_{FILM}$$

$$\cdot \bar{A}_R \int_{A_{FILM}} A_R A' e^{-i(\phi_L' + \omega_L t)} \; (-i) \int_{A_1} P_O e^{-i(\phi_O + \frac{2\pi}{\lambda_A} y \sin \theta_R)}$$

$$(1+e^{-i\Delta\phi_O}) \, dA_1 dA_{FILM} \tag{26}$$

or

$$I = A_R^4 (A')^2 \int_{FILM} \int_{A_1} P_O^2 \, (2) \, (1 + \cos \Delta\phi_O) \, dA_1 dA_{FILM} \tag{27}$$

and in expanded form

$$I = A_R^4 A^2 \frac{(128)}{\lambda_L^2} \pi^2 C_1^2 P_R^2 \int_{A_{FILM}} \int_{A_1} P_O^2 \, (1 + \cos \Delta\phi_O) \, dA_1 dA_{FILM} \tag{28}$$

Fringes occur when

$$\Delta\phi_O = \pi, \; 3\pi, \; 5\pi, \ldots \tag{29}$$

and are proportional to the object displacement. An experimental varification is needed. Because of the stability requirements of holography, it is questionable whether a hologram can be seen with the system isolation available.

Many attempts were made at getting a hologram. Some very faint single exposure holograms were recorded but were judged circumstantial in that the results could not be repeated. This is the kind of results that would suggest an unstable system.

To emphasize what one should expect from the focused acoustical holographic work, an optical focused image system was set up. Figure 5 shows the optical arrangement. Figure 6 is a reconstruction of the optical focused image hologram. Note that the optical reconstruction (Figure 7) uses a conjugate reference beam and is conditioned with a spatial filter and a telescopic lens system for intensity. The original lens opening focuses at a point and to see the image another lens is placed at this point and the image projected on a screen. The result is pictured in Figure 6. A double exposure focused image hologram of the same object is illustrated in Figure 8. The object was displaced between exposures. It is easily observed that the fringes and object do not focus in the same plane. Figure 9 illustrates a different target that was also displayed between exposures. In this example, the fringes are essentially in focus with the target.

In attempting to record the acoustical holographic information, the surface of the water was seen to move. A variation of Michelson's interferometer was set up with the acoustic holographic imaging system to check the stability of the system for the holographic records. Faint, transient fringes would occasionally be seen, suggesting that the system was not stable enough for holography. Next, a photodetector was placed in the image plane of the acoustic system to monitor the frequency of the observed motion. The frequency corresponded to the repetition rate of the pulse generator (250 Hz). The concept behind the repetition rate is to acoustically pulse the water surface then to have a quiet time so all reverberations can dissipate before the surface is pulsed again with 3 megahertzs, or whatever the desired frequency. This seems to account for at least some of the difficulty in getting a holographic record of the real-time acoustic hologram. It was anticipated that a continuous acoustic excitation would be more likely to produce a steady standing wave and so was potentially better for holographic recordings. This was tried. The arragnement used to control the pulses to the transducers did not have enough flexibility to properly tune the transducers and definite conclusions were unwarranted. However, it appears a continuous beam does not improve the stability of the waves.

Another possibility in overcoming the transient nature of the pulse acoustic waves for holography is to use a Q-switched ruby laser. By switching the ruby laser for say a hundred microseconds, the acoustic wave will appear stationary. The need for the ruby laser is to have enough intensity for exposure of the film with reduced time.

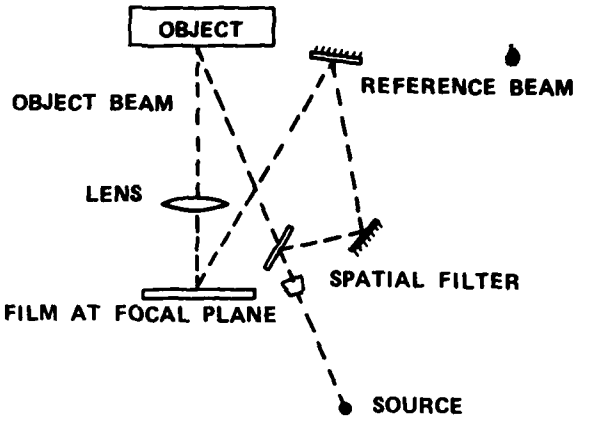

Figure 5. Optical arrangement for focused image holography.

Figure 6. Focused image hologram.

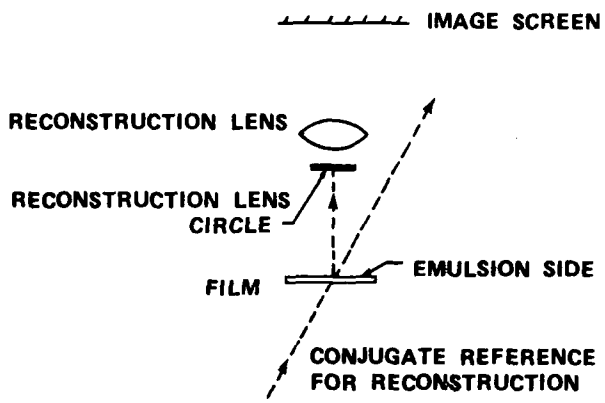

Figure 7. Focused image reconstruction.

Figure 8. Double exposed focused image hologram.

Figure 9. Double exposed focused image hologram - Example 2.

IV. ACOUSTICAL INTERFEROMETRY WITH YOUNG'S FRINGES

The acoustic object beam, being a coherent source, causes speckle on the surfaces of the object. It seems reasonable that the acoustic lens would image this acoustic speckle on the surface of the water. This imaged speckle would in turn modulate the reflected laser light so the real-time image of the object contains the acoustic speckle information and can be used to produce Young's fringes.

To describe this speckle effect, consider the speckle as projected on the water surface. Figure 10a represents an aperture on the water surface that vibrates relative to time and in the Z-direction. Figure 10b represents a true view of a plane passing through O and Q and along the Z-direction. Note that all points vibrate between the extremes of the dashed lines. The phase of point "O" is

$$\phi_O = (2)\ \left(\frac{2\pi}{\lambda_L}\right)\ Z_A(\sin\ \omega_A t)n \tag{30}$$

where

Z_A = the maximum height of the water surface,

n = direction cosine of the light rays passing through the aperture relative to the Z-axis.

The first (2) of Equation (30) accounts for the fact that in practice since the light reflects from the surface, the effective path length change is twice the height of the vibrating surface. The phase change of point Q at any instant is

$$\phi_Q = \phi_O - \frac{4\pi}{\lambda_L}\ (xl + my) \tag{31}$$

or

$$\phi_Q = \frac{4\pi}{\lambda_L}\ \left[Z_A n\ \sin\ \omega_A t - (xl + my)\right] \tag{32}$$

where l and m are the direction cosines of the light rays through the aperture relative to X and Y respectively. The optical disturbance at P is

$$\overline{E}_P = \int_0^t \int_{-\frac{b}{2}}^{b/2} \int_{-a/2}^{a/2} \overline{A}\ e^{i(\omega_L t + \frac{4\pi}{\lambda_L}\ n\ Z_A\ \sin\ \omega_A t\ -\ xl\ -\ my)}\ dxdydt\ . \tag{33}$$

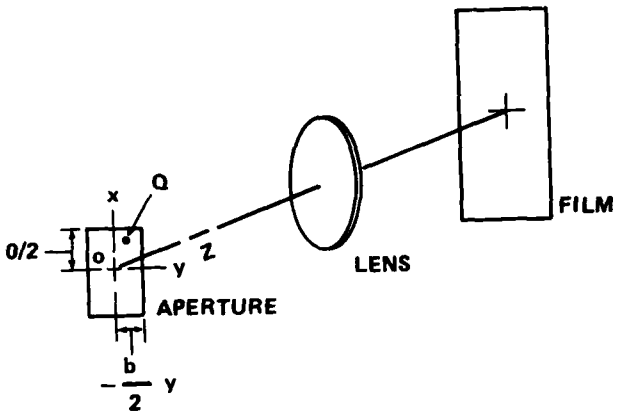

Figure 10a. Speckle arrangement.

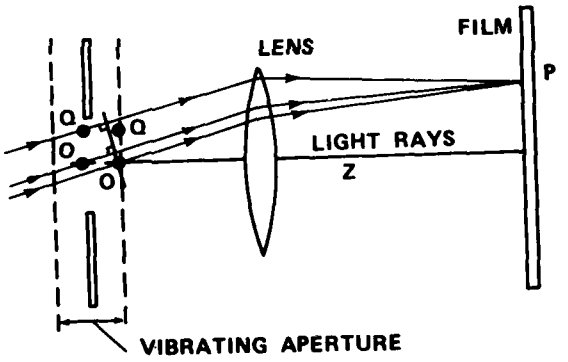

Figure 10b. Vibrating aperture.

Since light is a transverse vibration relative to time, the term $e^{i(\omega_L t)}$ can be removed outside the integral. Integrating with respect to X and Y reduces Equation (33) to

$$\bar{E}_P = \bar{A}\, e^{i\omega_L t}\left[\frac{a \sin(a\pi l/\lambda_L)}{(a\pi/\lambda_L)}\right]\left[\frac{b \sin(b\pi m/\lambda_L)}{(b\pi m/\lambda_L)}\right]$$

$$\int_o^t e^{i\frac{4\pi}{\lambda_L} nZ_A \sin \omega_A t}\, dt \quad . \tag{34}$$

Recall from Bessel Function analysis

$$2\pi\, J_O(X) = \int_0^{2\pi} e^{i(X)\cos\theta} d\theta = \int_0^{2\pi} e^{i(X)\sin\theta}\, d\theta \tag{35}$$

and let

$$\theta = \omega_A t$$

$$d\theta = \omega_A dt$$

$$X = \frac{4\pi}{\lambda_L} Z_A n$$

t = time for one cycle, $2\pi/\omega_A$, for multiple cycles the results are repeated,

thus

$$\bar{E}_P = \frac{A\, e^{i\omega_L t}}{\omega_A}\left[\frac{a \sin(a\pi l/\lambda_L)}{(a\pi l/\lambda_L)}\right]\left[\frac{b \sin(b\pi m/\lambda_L)}{(b\pi m/\lambda_L)}\right]$$

$$2\pi\, J_O\left(\frac{4\pi}{\lambda_L} Z_A n\right) \quad . \tag{36}$$

The intensity at P is

$$I_P = \frac{4\pi^2 A^2 a^2 b^2}{\omega_A^2}\left[\frac{\sin(a\pi l/\lambda_L)}{(a\pi l/\lambda_L)}\right]^2\left[\frac{\sin(b\pi m/\lambda_L)}{(b\pi m/\lambda_L}\right]^2\left[J_O\frac{(4\pi Z_A n)}{\lambda_L}\right]^2 \quad . \tag{37}$$

Each of the bracketed terms modulates the light intensity according to the graph shown in Figure 11. The curves are not identical but of the same general shape and visible light is expected near the central portion of the screen.

To examine what is expected when a double exposure is made of the speckle distribution as one pattern is shifted or deformed relative to the other, consider two nearby apertures of equal size, Figure 12. The aperture separation, u, is taken in the x direction for convenience. The optical disturbance at P due to light from the apertures is

$$\bar{E}_1 = \bar{A}\ ab\ \frac{e^{i(\omega_L t)}}{\omega_A}\left[\frac{\sin\ a\pi l/\lambda_L}{a\pi l/\lambda_L}\right]\left[\frac{\sin\ b\pi m/\lambda_L}{b\pi m/\lambda_L}\right]$$

$$2\pi\ J_0\left(\frac{4\pi}{\lambda_L}\ Z_A n\right)e^{i\phi_1} \tag{38}$$

and

$$\bar{E}_2 = \bar{A}\ ab\ \frac{e^{i\omega_L t}}{\omega_A}\left[\frac{\sin\ a\pi l/\lambda_L}{a\pi l/\lambda_L}\right]\left[\frac{\sin\ b\pi m/\lambda_L}{b\pi m/\lambda_L}\right] 2\pi\ J_0\left(\frac{4\pi}{\lambda_L}\ Z_A n\right)$$

$$e^{i(\phi_1\ -\ u\ 2\pi\ \sin\theta/\lambda_L)} \tag{39}$$

The intensity at P is

$$I_P = (\bar{E}_1 + \bar{E}_2)\cdot(\bar{E}_1 + \bar{E}_2)^* \tag{40}$$

or

$$I_P = \left(\frac{A\ ab\ 2\pi}{\omega_A}\right)^2\left[\frac{\sin\ \frac{a\pi l}{\lambda_L}}{\frac{a\pi l}{\lambda_L}}\right]^2\left[\frac{\sin\ \frac{b\pi m}{\lambda_L}}{\frac{b\pi m}{\lambda_L}}\right]^2 J_0^2\ \frac{(4\pi Z_A n)}{\lambda_L}$$

$$4\ \cos^2\left(\frac{\pi u\ \sin\ \theta}{\lambda_L}\right). \tag{41}$$

The interpretation of Equation (41) is a halo of light determined by the two bracket terms and the Bessel term with fringes occurring within the halo (Reference Technical Report T-78-5, US Army Missile Research and Development Command, 26 Sept 1977). Inspecting the cosine term which causes the fringes, it is apparent the fringes occur when the intensity goes to zero, or when

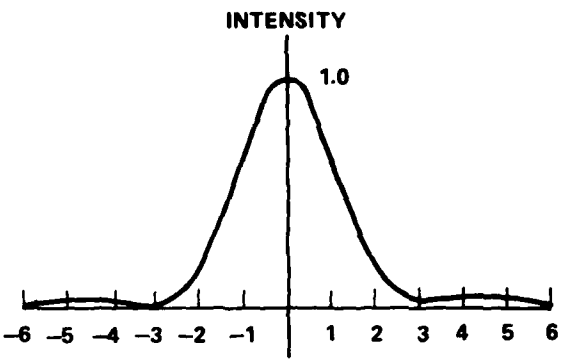

Figure 11. Intensity distribution.

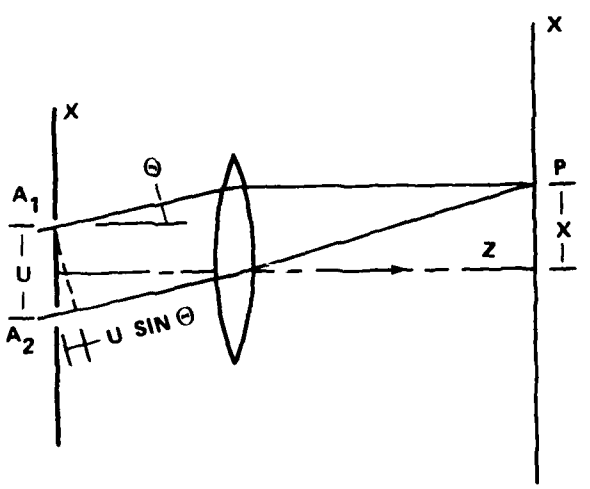

Figure 12. Two nearby apertures.

$$u = \frac{\lambda}{2 \sin \theta} \simeq \frac{\lambda f}{2X} \quad , \tag{42}$$

or

$$u = \pm \frac{2m_1 - 1}{2} \frac{\lambda f}{X} \text{ for } m_1 = 1,2,3, \ldots$$

where

f = focal distance of lens.

Because the rectangular aperture is an assumed shape, it is noted that the Bessel term is more definite than are the other terms effecting the halo size. This will be discussed more later in the report.

Many attempts were made at recording an acoustic specklegram. A sandwich procedure was tried and produced significant results. The concept behind the sandwich technique is to increase the range of sensitivity for making specklegrams. First, the object speckle is photographed through a blank piece of film glass. A second photograph of the speckle reflecting off the water surface is taken with a second glass-backed film. In the second photograph, the speckle wave front came through the glass back and then activated the emulsion. For observation, instead of a double exposure on a single film, the two films were sandwiched together with the emulsions in contact. The two are mechanically moved until the two speckle patterns correlate and Young's fringes are observed. One advantage of this procedure is when an object moves more than 0.02 inch between exposures, the negatives can still be correlated for Young's fringes while this would be impossible with a double-exposed single negative. There are limits to the amount of shift possible and still have the negatives correlate but the range of sensitivity is increased. Further engineering problems occur where there is not enough displacement for Young's fringes to be observed using a single double-exposed negative. With the sandwich technique one negative can be shifted relative to the other and fringes observed, this time extending the range of sensitivity below the usual minimum of a double-exposed single negative. The sandwich technique is most applicable in evaluating strain as the imposed rigid body motion of one film moving relative to the other is of no consequence. Theory has been written for this technique and is reported in "Development of Basic Theories and Techniques for Determining Stresses in Rotating Turbine or Compressor Blades" by C. H. Chien, W. F. Swinson, J. L. Turner, F. A. Moslehy, W. F. Ranson, Auburn University Engineering Experiment Station, Final Report NSG-3233, May 1980.

Using the real-time beam that images the acoustic hologram from the water surface, sandwich specklegrams were made and very distinct fringes were observed as shown in Figure 13. By shifting one negative relative to the other the orientation and spacing of the fringes change as, of course, would be expected. Figure 14 is made with the same negatives as Figure 13 but with one negative shifted still further relative to the other. Figure 15 shows the same negatives as used in Figures 13 and 14 but in perfect alignment and no fringes are seen. It is observed that the halo is not circular as is the case with usual specklegrams. The cause of this halo change seems to be

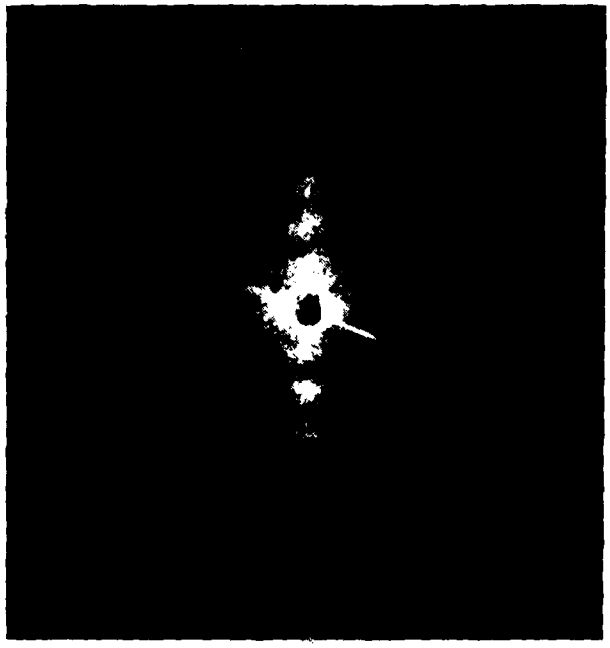

Figure 13. Acoustic Young's fringes - Example 1.

Figure 14. Acoustic Young's fringes - Example 2.

because of the vibrating water surface and has been ovserved before with time average specklegrams of vibrating objects. The Bessel term, Equation (41), in the analytical description may help explain this, but more thought is needed here. Other differences were observed with acoustic specklegrams. Figure 16 shows a vertical long narrow halo and a very bright horizontal smaller halo is also evident. This small bright halo is evident on most of the acoustic specklegrams taken and in some cases was the only halo observed. Fringes in the vertical halo appear to extend into the horizontal halo. Figure 17 is a sandwich specklegram in which there was approximately 0.005 inch displacement of the object between exposures. The correlation even with displacement of the object is apparent. It is very evident from this film record that acoustic speckle can be used to monitor displacements of objects, and more importantly has the capability to establish strain distributions of an object under load.

Some work was done to try and establish the effect of different surface roughness conditions and the effect on acoustic speckle. While surface roughness is a variable, the effects of film exposure and stability of the acoustic system overshadowed conclusions on the surface effects at this point.

V. REAL-TIME ACOUSTICAL HOLOGRAPHY SYSTEM

To improve the imaging capabilities of the acoustical holography system detergent was added to the water in the immersion tank. The prupose was to reduce the surface tension of the water. With reduced surface tension the acoustic signals would have a greater rippling effect. The result was significant and is illustrated in Figures 18 - 20. Figure 18 shows a metal rod imbedded in an epoxy piece that also has a hole in it; Figure 19 illustrates a piece of fiberboard with a hole in it and covered with a plastic case; Figure 20 is a model of a steel and silica sandwich with a Teflon flaw between the two materials.

VI. SUMMATION

1. A theory has been written that seems sufficient to describe real-time acoustical holography.

2. A theory has been written that describes a technique for recording the real-time acoustic holographic information with an optical hologram. This technique presents the potential for a double exposed hologram to evaluate displacements of the insonified object. This would apply in principle to interior planes as well as surface planes of the object; thus, conceivably interior and surface strains could be calculated.

3. A description of double-exposed focused image holography is presented to assist in developing the potential of optical holographic recording of the acoustical holographic information noted in item 2 above.

4. A theory for using acoustic speckle for evaluating displacements of an insonified object has been written.

5. A sandwich technique for recording acoustic speckle has been described and demonstrated. With this procedure strains of insonified objects can be calculated.

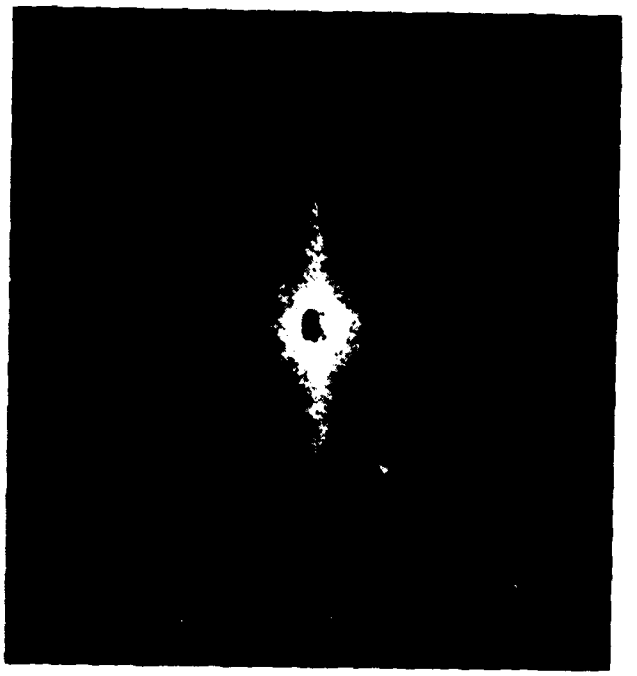

Figure 15. Acoustic halo.

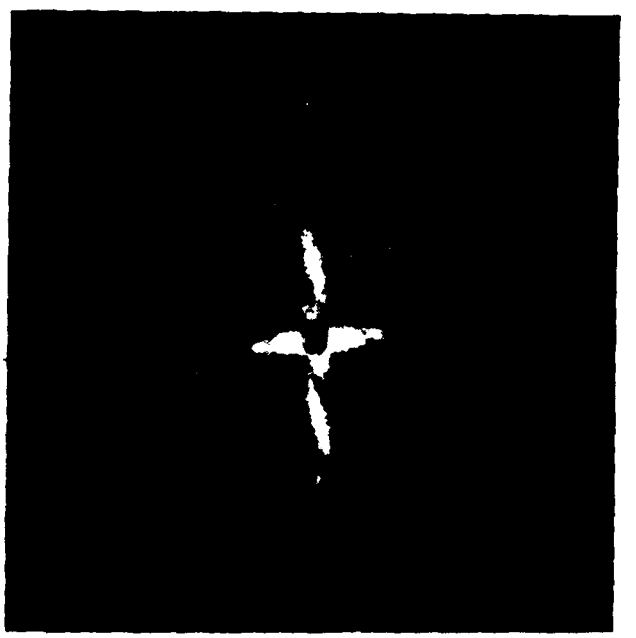

Figure 16. Two acoustic halos.

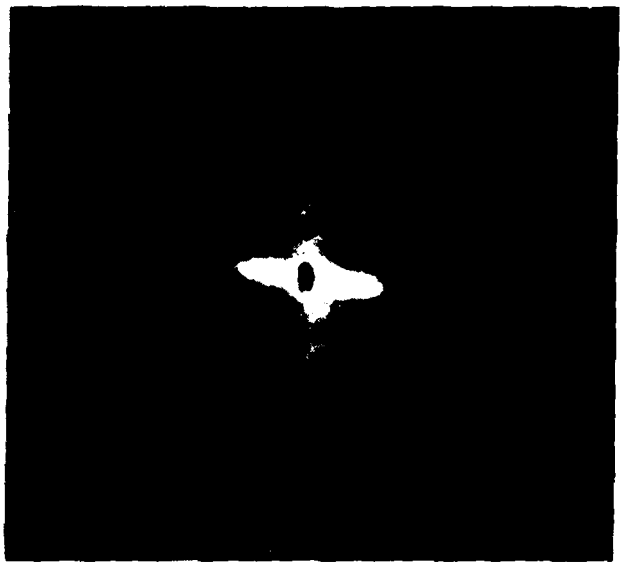

Figure 17. Acoustic Young's fringes - Example 3.

Figure 18. Acoustic hologram - Example 1.

6. For real-time acoustic holography the rippling effect of the ultrasonic signals can be amplified by adding detergent to the water immersion fluid.

VII. RECOMMENDATIONS

1. It is recommended that work continue on recording the acoustic holographic information with optical holography. In particular, stabilizing the system is needed. Some damping procedures would help. More examination of continuous waves as a means of getting a standing wave is warranted. The use of a pulse laser is the most likely way to, in effect, stabilize the system. The potential of this holographic recording technique is important in that it can quantify the whole field of acoustic signals making it possible to calculate strains and stresses in an object.

2. It is recommended that work continue on the use of acoustic speckle for monitoring displacements of objects. Some stabilization of the system is needed, though not as much as with the above holographic technique. An example problem where the strain field is determined using acoustic speckle to produce Young's fringes is needed.

3. To improve the image quality real-time acoustic holograms, some enhancement through filtering of the data is needed. This can be accomplished through a videcon camera, a computer and some programming,all of which would need adapting and/or developing. There are commercial units available (for example from the Quantex Corporation) that have developed the complete system to do this type of image enhancement. Further, there is the possibility of doing interferometry work with such units.

4. More work is needed with the addition of soap to amplify the acoustic signal effect. Questions such as how much soap is desired, and will the signal amplification effect improve the speckle or holographic technique need answering. Incidentally, the soap does reduce the amount of rust on components in the tank.

Figure 19. Acoustic hologram - Example 2.

Figure 20. Acoustic hologram - Example 3.

DISTRIBUTION

	No. of Copies
Director USA Mobility Equipment Research and Development Center Coating and Chemical Laboratory ATTN: STSFB-CL Aberdeen Proving Ground, Maryland 21005	1
Commander Edgewood Arsenal ATTN: SAREA-TS-A Aberdeen Proving Ground, Maryland 21010	1
Commander Picatinny Arsenal ATTN: SARPA-TS-S, Mr. M. Costello Dover, New Jersey 07801	1
Commander Rock Island Arsenal Research and Development ATTN: 9320 Rock Island, Illinois 61201	1
Commander Watervliet Arsenal Watervliet, New York 12189	1
Commander US Army Aviation Systems Command ATTN: DRSAV-EE -MT, Mr. Vollmer St. Louis, Missouri 63166	1 1
Commander US Army Aeronautical Depot Maintenance Center (Mail Stop) Corpus Christi, Texas 78403	1
Commander UA Army Test and Evaluation Command ATTN: DRSTE-RA Aberdeen Proving Ground, Maryland 21005	1
Commander ATTN: STEAP-MT Aberdeen Proving Ground, Maryland 21005	1

DISTRIBUTION (CONTINUED)

	No. of Copies
Chief Bureau of Naval Weapons Department of the Navy Washington, DC 20390	1
Chief Bureau of Ships Department of the Navy Washington, DC 20315	1
Naval Research Laboratory ATTN: Dr. M. M. Krafft Code 8430 Washington, DC 20375	1
Commander Wright Air Development Division ATTN: ASRC Wright-Patterson AFB, Ohio 45433	1
Director Army Materials and Mechanics Research Center ATTN: DRXMR-PL -MT, Mr. Farrow Watertown, Massachusetts 02172	1 1
Commander White Sands Missile Range ATTN: STEWS-AD-L White Sands Missile Range, New Mexico 88002	1
Jet Propulsion Laboratory California Institute of Technology ATTN: Library/Acquisitions 111-113 4800 Oak Grove Drive Pasadena, California 91103	1
Sandia Laboratories ATTN: Library P. O. Box 969 Livermore, California 94550	1
Commander US Army Air Defense School ATTN: ATSA-CD-MM Fort Bliss, Texas 79916	1

DISTRIBUTION (CONTINUED)

	No. of Copies
Technical Library Naval Ordnance Station Indian Head, Maryland 20640	1
Commander US Army Materiel Development and Readiness Command ATTN: DRCMT Washington, DC 20315	1
Headquarters SAC/NRI (Stinfo Library) Offutt Air Force Base, Nebraska 68113	1
Commander Rock Island Arsenal ATTN: SARRI-KLPL-Technical Library Rock Island, Illinois 61201	1
Commander (Code 233) Naval Weapons Center ATTN: Library Division China Lake, California 93555	1
Department of the Army US Army Research Office ATTN: Information Processing Office P. O. Box 12211 Research Triangle Park, North Carolina 27709	1
Commander US Army Research Office ATTN: DRXRO-PW, Dr. R. Lontz P. O. Box 12211 Research Triangle Park, North Carolina 27709	2
US Army Research and Standardization Group (Europe) ATTN: DRXSN-E-RX, Dr. Alfred K. Nodoluha Box 65 FPO New York 09510	2
Headquarters Department of the Army Office of the DCS for Research Development and Acquisition ATTN: DAMA-ARZ Washington, DC 20310	2
Director Air Force Materiel Laboratory ATTN: AFML-DO-Library Wright-Patterson AFB, Ohio 45433	1

DISTRIBUTION (CONCLUDED)

	No. of Copies
US Army Materiel Systems Analysis Activity ATTN: DRXSY-MP Aberdeen Proving Ground, Maryland 21005	1
IIT Research Institute ATTN: GACIAC 10 West 35th Street Chicago, Illionis 60616	1
ADTC (DLDSL) Eglin Air Force Base, Florida 32542	1
University of California Los Alamos Scientific Laboratory ATTN: Reports Library P. O. Box 1663 Los Alamos, New Mexico 87545	1
Commander US Army Materiel Development and Readiness Command ATTN: DRCRD DRCDL 5001 Eisenhower Avenue Alexandria, Virginia 22333	1 1
Director Defense Advanced Research Projects Agency 1400 Wilson Boulevard Arlington, Virginia 22209	1
DRSMI-LP, Mr. Voigt	1
R, Dr. McCorkle	1
RL, Mr. Comus	1
RLA, Mr. Pettey	1
RLA, Mr. Schaeffel	50
RPR	15
RPT, Record	1
RPT, Reference	1

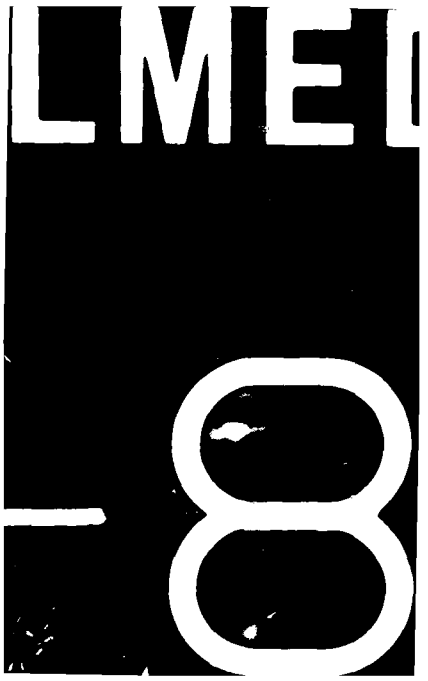
LMEL
8